REPORT DOCUMENTATION PAGE

Form Approved OMB NO. 0704-0188

1. REPORT DATE (DD-MM-YYYY)	2. REPORT TYPE	3. DATES COVERED (From - To)
02-12-2018	Final Report	1-Feb-2014 - 31-Jan-2017

4. TITLE AND SUBTITLE
Final Report: Electrochemistry of Nanostructured Carbon Electrodes in Room-Temperature Ionic Liquids

5a. CONTRACT NUMBER
W911NF-14-1-0063

5b. GRANT NUMBER

5c. PROGRAM ELEMENT NUMBER
611102

6. AUTHORS

5d. PROJECT NUMBER

5e. TASK NUMBER

5f. WORK UNIT NUMBER

7. PERFORMING ORGANIZATION NAMES AND ADDRESSES
Michigan State University
Hannah Administration Building
426 Auditorium Road, Room 2
East Lansing, MI 48824 -2600

8. PERFORMING ORGANIZATION REPORT NUMBER

9. SPONSORING/MONITORING AGENCY NAME(S) AND ADDRESS (ES)
U.S. Army Research Office
P.O. Box 12211
Research Triangle Park, NC 27709-2211

10. SPONSOR/MONITOR'S ACRONYM(S)
ARO

11. SPONSOR/MONITOR'S REPORT NUMBER(S)
63160-CH.11

12. DISTRIBUTION AVAILIBILITY STATEMENT
Approved for public release; distribution is unlimited.

13. SUPPLEMENTARY NOTES
The views, opinions and/or findings contained in this report are those of the author(s) and should not contrued as an official Department of the Army position, policy or decision, unless so designated by other documentation.

14. ABSTRACT

15. SUBJECT TERMS

16. SECURITY CLASSIFICATION OF:			17. LIMITATION OF ABSTRACT	15. NUMBER OF PAGES	19a. NAME OF RESPONSIBLE PERSON
a. REPORT	b. ABSTRACT	c. THIS PAGE			Greg Swain
UU	UU	UU	UU		19b. TELEPHONE NUMBER 517-353-1090

RPPR Final Report
as of 27-Dec-2018

Agency Code:

Proposal Number: 63160CH **Agreement Number: W911NF-14-1-0063**
INVESTIGATOR(S):

Name: Ph.D. Greg M. Swain
Email: swain@chemistry.msu.edu
Phone Number: 5173531090
Principal: Y

Organization: **Michigan State University**
Address: Hannah Administration Building, East Lansing, MI 488242600
Country: USA
DUNS Number: 193247145 EIN: 386005984
Report Date: 28-Feb-2015 Date Received: 02-Dec-2018
Final Report for Period Beginning 01-Feb-2014 and Ending 31-Jan-2017
Title: Electrochemistry of Nanostructured Carbon Electrodes in Room-Temperature Ionic Liquids
Begin Performance Period: 01-Feb-2014 **End Performance Period:** 30-May-2018
Report Term: 0-Other
Submitted By: Ph.D. Greg Swain Email: swain@chemistry.msu.edu
Phone: (517) 353-1090

STEM Degrees: 2 **STEM Participants:** 8

Major Goals: Fundamental research was conducted to better understand factors governing redox reactions and the interfacial organization at nanostructured boron-doped diamond (BDD) and nitrogen-incorporated tetrahedral amorphous carbon (ta-C:N) thin-film electrodes in room temperature ionic liquids (RTILs) andaqueous electrolyte solutions. The major goals of the research project were to increase knowledge about how the surface microstructure, surface chemistry and bulk electronic properties of these nanostructured carbon electrodes affect (i) heterogeneous electron-transfer rate constants for soluble redox systems and (ii) voltammetric background current and potential-dependent capacitance. Additionally, we took advantage of the excellent properties of these new electrodes (low background current, wide working potential window, resistance to fouling, etc.) and developed electrochemical detection assays for several environmental and biological analytes. The research was organized around three specific aims. Specific Aim 1 involved detailed characterization of the morphology, microstructure, doping level and chemical composition (bulk and surface) of the different carbon materials enabling correlations to be made with the electrochemical properties. Specific Aim 2 involved cyclic voltammetric studies of various soluble redox systems in RTILs at the two types of nanostructured carbon electrodes, as a function of the RTIL type and temperature, to determine heterogeneous electron-transfer rate constants and activation energies for electron transfer. Comparison studies were performed in aqueous electrolytes. Specific Aim 3 focused on using voltammetric methods and electrochemical impedance spectroscopy to learn how the surface microstructure and chemistry affect potential-dependent capacitance at the two carbon electrode materials as a function of the RTIL type. Again, comparison studies were performed in aqueous electrolyte solutions.

Accomplishments: See uploaded Final Report

RPPR Final Report
as of 27-Dec-2018

Training Opportunities: This research project provided scientific training and professional development for 6 PhD graduate and undergraduate students and 2 high school students. Two of the undergraduates and high school students were AEOP fellows. The research will produce new knowledge about the physical, chemical and electrical properties of nanostructured diamond carbon materials useful for a range of electrochemical applications beneficial to human health and the environment. Knowledge and practices gained from the project's interdisciplinary research agenda provided students with the tools needed to be successful scientists. Students developed improved critical thinking and communication skills, and learned how to productively interact with colleagues in a laboratory setting. Professional development activities gave the students (graduate, undergraduate and high school) confidence and make them more competitive for employment, graduate school or undergraduate studies in STEM. The high school and undergraduate student participants experienced graduate level research and training at a formative point in their careers, enhancing their desire to enter graduate school and ultimately become professional scientists. Finally, the students experienced the benefit of positive mentoring . The research served to train our next-generation of electrochemists and material scientists.

Results Dissemination: The results of the research project were disseminated through publications in peer-reviewed publications, presentations and scientific meetings and conferences, and presentations to smaller groups of prospective graduate and undergraduate students.

Honors and Awards: Honors received by the PI during the period:
Guest Professorship, Keio University (Japan), Faculty of Science and Technology, 2018-2019
Academic Advancement Network Leadership Fellow, Michigan State Univ., 2018-2019
NatSci Outstanding Faculty Award, Michigan State University, 2018-2019
Fulbright Scholar Award (Carbon Electrodes and Electrochemistry) – Ecuador 2018-2020
Fulbright Specialist Award (Diamond and Diamond-Like Carbon Electrodes) – Czech Rep. 2018

Honors received by the students during the period:
Travel Grants from the MSU Graduate School and the Council of Graduate Students

Protocol Activity Status:

Technology Transfer: No interactions with DOD laboratories so far on this project.

G. M. Swain, S. Peteu and B. Hrinczenko, "Electrode and Sensor Apparatus and Related Methods for Detection of Nitric Oxide and Peroxynitrite", Patent No. US2018217087-A1(February 1, 2018).

PARTICIPANTS:

Participant Type: PD/PI
Participant: Greg M Swain
Person Months Worked: 1.00 **Funding Support:**
Project Contribution:
International Collaboration:
International Travel:
National Academy Member: N
Other Collaborators:

Participant Type: Graduate Student (research assistant)
Participant: Romana Jarosova
Person Months Worked: 12.00 **Funding Support:**
Project Contribution:
International Collaboration:
International Travel:
National Academy Member: N
Other Collaborators:

Participant Type: Graduate Student (research assistant)

RPPR Final Report
as of 27-Dec-2018

Participant: Kirti Bhardwaj
Person Months Worked: 12.00 **Funding Support:**
Project Contribution:
International Collaboration:
International Travel:
National Academy Member: N
Other Collaborators:

Participant Type: Graduate Student (research assistant)
Participant: Maria Navarez Espinosa
Person Months Worked: 6.00 **Funding Support:**
Project Contribution:
International Collaboration:
International Travel:
National Academy Member: N
Other Collaborators:

Participant Type: Graduate Student (research assistant)
Participant: Victoria Perugachi
Person Months Worked: 6.00 **Funding Support:**
Project Contribution:
International Collaboration:
International Travel:
National Academy Member: N
Other Collaborators:

Participant Type: Graduate Student (research assistant)
Participant: Elizabeth Espinosa
Person Months Worked: 6.00 **Funding Support:**
Project Contribution:
International Collaboration:
International Travel:
National Academy Member: N
Other Collaborators:

Participant Type: High School Student
Participant: Maggie Gajda
Person Months Worked: 3.00 **Funding Support:**
Project Contribution:
International Collaboration:
International Travel:
National Academy Member: N
Other Collaborators:

Participant Type: Undergraduate Student
Participant: Sandra Mcclure
Person Months Worked: 6.00 **Funding Support:**
Project Contribution:
International Collaboration:
International Travel:
National Academy Member: N
Other Collaborators:

RPPR Final Report
as of 27-Dec-2018

Participant Type: Graduate Student (research assistant)
Participant: Vanessa Maldonado
Person Months Worked: 6.00 **Funding Support:**
Project Contribution:
International Collaboration:
International Travel:
National Academy Member: N
Other Collaborators:

Participant Type: High School Student
Participant: Monica Davis
Person Months Worked: 3.00 **Funding Support:**
Project Contribution:
International Collaboration:
International Travel:
National Academy Member: N
Other Collaborators:

PATENTS:

Intellectual Property Type: Patent Date Received:
Patent Title: Electrode and Sensor Apparatus and Related Methods for Detection of Nitric Oxide and Peroxynitrite
Patent Abstract: The disclosure relates to electrodes and related sensor apparatus for the detection of nitric oxid
Patent Number: US2018217087-A1
Patent Country: USA
Application Date: 01-Feb-2017 Application Status: 3
Date Issued:

Final Report (February 2014 - June 2018)

Fundamental research was conducted to better understand factors governing redox reactions and the interfacial organization at nanostructured boron-doped diamond (BDD) and nitrogen-incorporated tetrahedral amorphous carbon (t*a*-C:N) thin-film electrodes in room temperature ionic liquids (RTILs) andaqueous electrolyte solutions. The major goals of the research project were to increase knowledge about how the surface microstructure, surface chemistry and bulk electronic properties of these nanostructured carbon electrodes affect (i) heterogeneous electron-transfer rate constants for soluble redox systems and (ii) voltammetric background current and potential-dependent capacitance. Additionally, we took advantage of the excellent properties of these new electrodes (low background current, wide working potential window, resistance to fouling, etc.) and developed electrochemical detection assays for several environmental and biological analytes. The research was organized around three specific aims. **Specific Aim 1** involved detailed characterization of the morphology, microstructure, doping level and chemical composition (bulk and surface) of the different carbon materials enabling correlations to be made with the electrochemical properties. **Specific Aim 2** involved cyclic voltammetric studies of various soluble redox systems in RTILs at the two types of nanostructured carbon electrodes, as a function of the RTIL type and temperature, to determine heterogeneous electron-transfer rate constants and activation energies for electron transfer. Comparison studies were performed in aqueous electrolytes. **Specific Aim 3** focused on using voltammetric methods and electrochemical impedance spectroscopy to learn how the surface microstructure and chemistry affect potential-dependent capacitance at the two carbon electrode materials as a function of the RTIL type. Again, comparison studies were performed in aqueous electrolyte solutions.

Specific Aim 1. Material Characterization of the Different Diamond and Diamond-Like Carbon Thin-Film Electrodes.

The goal of this aim was to characterize the physical, chemical and electronic properties of BDD and ta-C:N thin-film electrodes. Material characterization is critically important for understanding how the material properties correlate with the electrochemical behavior.

The BDD and t*a*-C:N electrodes offer some superlative properties for electrochemical measurements including unprecedented robustness, detection capability, fouling resistance, biocompatibility and corrosion/degradation resistance in complex environments. Detailed studies were completed of boron-doped nanocrystalline diamond films deposited on conducting Si and quartz. As an example, the morphology, microstructure, chemistry and electronic properties of a boron-doped nanocrystalline diamond (BDD) thin film grown on quartz, a so-called optically transparent diamond electrode, are summarized here. Diamond optically transparent electrodes (OTEs) are useful for transmission spectroelectrochemical measurements offering excellent stability during anodic and cathodic polarization and exposure to a variety of chemical environments. Detailed characterization of this and other BDD and t*a*-C:N films was performed using AFM, optical spectroscopy, Raman spectroscopic mapping, AC Hall Effect measurements and XPS. Similar material properties were found for nanocrystalline diamond films deposited on Si.

The following conclusions were reached about the diamond deposited on quartz.

1. Thin and continuous diamond thin-film optically transparent electrodes can be grown on quartz with good adhesion and uniform film thickness with proper substrate pretreatment. The mechanical polishing and ultrasonic seeding pretreatment used produces a high initial nucleation density that leads to a continuous nanocrystalline film without grain coarsening in a short growth period.
2. The nanocrystalline diamond film consists of primary grains that are 60-85 nm in diameter after a 2-h growth. The film exhibits *ca.* 60 % optical transparency from 350-600 nm.
3. The microstructure of the diamond OTE is uniform across the surface, as evidenced by the Raman mapping. The spectral features reflect the nanocrystalline morphology of the film, the relatively high fraction of grain boundaries, and the substitutional insertion and clustering of boron dopant atoms. Additionally, the spectral features are characteristic of a heavily boron-doped film.
4. Temperature-dependent Hall Effect measurements revealed a room temperature resistivity of 0.06 Ω cm

that decreases by only a factor of 2 during a temperature ramp from 300 to 700 K. The carrier concentration, *ca.* 10^{21} cm^{-3}, and carrier mobility, *ca.* 0.2 cm^2 V^{-1} s^{-1}, were largely temperature independent, consistent with the electronic properties of a degenerate semiconductor or semimetal. A low activation energy of conduction of 10 meV was determined.

5. XPS revealed a surface low in carbon-oxygen functionalities, O/C = 0.03. The boron doping level was uniform with depth into the film. The boron concentration *ca.* 10^{21} cm^{-3} in the film is consistent with the high boron doping level reflected in the Raman spectral features and with the high carrier concentration determined from Hall Effect measurements. The boron exists in three chemical environments: B-B pairs or clusters likely in grain boundaries, B-C groups due to the substitutional-inserted boron dopant atoms in the film, and B-O groups at the film surface.

Quasireversible electron-transfer kinetics were observed for multiple redox systems at 100-500 mV s^{-1}. The semi-metallic electrode material possesses a high density of electronic states over the entire potential range covered (~ 2V) by the redox analytes. All the redox systems exhibited diffusion-controlled behavior at the BDD OTE without any conventional pretreatment. Overall, the BDD OTE exhibits a high level of electrochemical activity. The diamond OTE is characterized by a low double-layer capacitance in both aqueous and ionic liquid media. Capacitance values of 2-7 μF cm^{-2} were recorded in H_2SO_4 and 0.7-1 μF cm^{-2} in [BMIM][BF_4]. The 5-6x lower capacitance at all potentials in the RTIL is consistent with the 5.5x lower dielectric constant.

Research was also conducted to fully characterize the morphology, microstructure and chemical composition of nitrogen-incorporated tetrahedral amorphous carbon thin-film electrodes. Films with different nitrogen content were characterized and used in this work. XPS is one tool used to determine the C, O and N content in the films. The t*a*-C:N films used were 200-300 nm thick. Figure 1A shows an XPS survey scan for a t*a*-C:N film deposited with 30 sccm N_2. Three major peaks are present for C1s (285.0 eV), N1s (395.0 eV) and O 1s (532.6 eV). The O/C atomic ratio was 0.162 and the N/C atomic ratio was 0.094 in this particular film. These determinations are based on known sensitivity factors for C, O and N. This film was exposed to the atmosphere for a lengthy period of time prior to the analysis so this is the reason for the relatively high O/C ratio. It is likely that the t*a*-C:N films will pick up oxygen over time when exposed to the atmosphere. A shown below, this oxygen exists in the near surface region of the film and not the bulk. The C1s spectrum is asymmetrically shaped with broadening on the high energy side of the peak due to the presence of C-O and C-N functional groups. The C1s peak was fit to four components: 284.66 eV (65.6 % area), 285.91 eV (24.8 % area), 287.46 eV (6.4 % area) and 288.65 eV (3.3 % area). The 284.66 eV peak is assumed to be associated with sp^2 bonded carbon (*e.g.*, graphite) and the 285.91 eV peak is assumed to be associated with sp^3 bonded carbon (*e.g*. diamond). The sp^3 carbon was estimated to be 25 %. This is lower than the 38% content determined from the Young's modulus. The XPS method for estimating the sp^3 carbon content is most accurate when there is little C1s peak area from higher binding energy components arising from surface functional groups (*i.e.*, carbon-oxygen). For this film, about 10%

of the total C1s peak area was associated with these functional groups. Therefore, it is supposed that the 25% sp^3 carbon content is an underestimate and it is probably closer to the 38 % value, or greater. Typically, the sp^3 carbon content in the t*a*-C:N film used as electrodes is 45-60 %.

The N1s peak was deconvoluted and fit to three components with the following areas: 398.56 (39.1%),

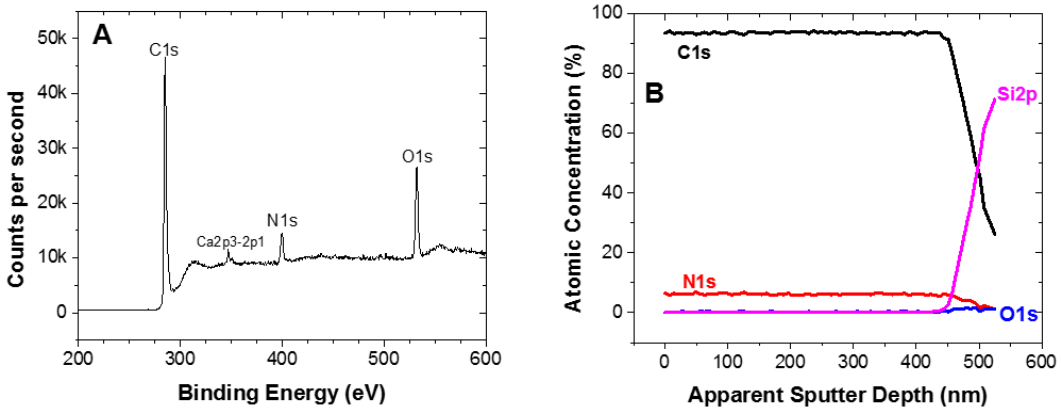

Figure 1. XPS (A) survey spectrum for a t*a*-C:N thin film deposited on a Si substrate in the presence of 30 sccm N_2 and (B) depth profiling data for C1s, O1s, N1s and Si2p through the film. Ar^+ sputtering at 4 kV was used for the profiling.

399.91 (52.7 %) and 401.41 (8.2 %). This result suggests that the N in the film exists in three different chemical environments. The peaks are assigned to N bonded to sp^3 carbon (398.56 eV), CN triple bonds (399.91 eV) and N-sp^2 carbon (401.41 eV). By way of comparison, peak at 398.6 eV has been assigned to pyridinic-like N and the peak at 401.8 eV to graphitic N in nitrogen-doped carbon nanotubes.

Figure 1B shows XPS depth profiles recorded for the t*a*-C:N film using 4 kV Ar^+ sputtering. The sputter depth is apparent but this particular film appears to be thicker than most others deposited under these conditions, *ca.* 200 nm. The C atomic concentration is constant with depth at about 93%. The Si concentration begins to increase once the substrate is reached. The N atomic concentration is constant at ~6 % through the film. The O atomic concentration is less than 1% through the film. These results indicate that the nitrogen content is relatively constant with depth in the t*a*-C:N film. The 6% atomic concentration corresponds to ~60,000 ppm (6 at.% = 10,000 ppm) or 2.6 x 10^{21} atoms N cm^{-3}. One overall goal of this and all the characterization work is to use tools that can provide spatial and depth information about the microstructure and chemical composition (doping level).

Specific Aim 2. **Heterogeneous Electron-Transfer Kinetics and Activation Energies for Electron Transfer for Soluble Redox Systems at the Different Carbon Electrodes in RTILs and Aqueous Electrolytes.**
The goal of this aim was to correlate the physical and chemical properties of BDD and ta-C:N thin-film electrodes with the electron-transfer kinetics and activation energies for electron transfer for various redox systems in RTILs and aqueous electrolyte solutions.

Heterogeneous electron-transfer rate constants were determined for several redox systems at BDD, t*a*-C:N and glassy carbon. Cyclic voltammetry was used to investigate the background current response as a function of potential, scan rate and electrolyte composition. Cyclic voltammetry and digital simulation were used to determine the heterogeneous electron-transfer rate constants (k^o) for $IrCl_6^{2-/3-}$, $Fe(CN)_6^{3-/4-}$, ferrocene carboxylic acid, $Ru(NH_3)_6^{3+/2+}$ and methyl viologen. The results revealed that the background current for

the t*a*-C:N electrode falls between that of BDD and GC. k^o values for all the redox analytes at t*a*-C:N were comparable to the values at BDD and GC. k^o values were lower for $Fe(CN)_6^{3-/4-}$, 10^{-3} cm s^{-1}, than for the other four redox systems, 10^{-2}-10^{-1} cm s^{-1}. k^o for $Ru(NH_3)_6^{3+/2+}$ was insensitive to the electrolyte cation (Li^+, Na^+, K^+ and Cs^+) at all three electrodes. In contrast, k^o for $Fe(CN)_6^{3-/4-}$ was sensitive to the cation type with the greatest sensitivity seen for the t*a*-C:N electrode suggestive of more significant double layer effects. The t*a*-C:N electrode supports relatively rapid electron transfer for a wide range of redox systems with formal potentials from ca. 0.9 to -1.0 V vs. Ag/AgCl.

We attempted to use these same highly charged inorganic redox systems, and others, to probe surface microstructure and chemistry effects on electron-transfer kinetics at the different carbon electrodes in RTILs. Unfortunately, these efforts did not produce meaningful results. It turns out that when a highly charged analyte, (*e.g.* $Fe(CN)_6^{3-/4-}$) is dissolved in an RTIL (*e.g.*, [BMIM][BF_4]), there is no electron transfer observed with the electrode. There is capacitive current but no faradaic response. This was observed for an electrode that exhibited a near-Nernstian response for the same redox system in 1 M KCl (0.1 V/s). There is apparently a very large reorganizational barrier to overcome for electron transfer to occur between the electrode and a charged redox system in a highly charged RTIL. In other words, there appears to be considerable reorganization energy necessary to rearrange RTIL ions organized around a charged redox system upon electron transfer. The large reorganizational energy barrier results in a very small k^o value. Such inactivity was seen for anionic and cationic redox systems, like $Fe(CN)_6^{3-/4-}$ and $Ru(NH_3)_6^{3+/2+}$. If small amounts of water are titrated into the RTIL, the electron transfer for these redox systems is regained in a manner that scales with the water content. Adding the dielectric water apparently helps to reduce the electrostatic attraction between the RTIL ions and the charged analyte. This lowers the activation barrier such that electron-exchange with the electrode at relatively low overpotentials can be observed. Therefore, the majority of the work conducted made use of ferrocene and ferrocene carboxaldehyde (neutral), ferrocene carboxylic acid (anion) and (ferrocenylmethyl)trimethylammonium iodide (cation). All of these (except ferrocene) undergo electron transfer with the electrodes in both aqueous electrolyte solutions and RTILs.

Figure 2 shows example data for 0.5 mM ferrocene carboxylic acid (FCA) in [BMIM][BF_4] at 0.3 V/s as a function of the temperature from 25-65 °C. The data were recorded at a t*a*-C:N electrode (30 sccm N_2). As the temperature is increased, the peak currents increase due to a lowering of the RTIL viscosity (*i.e.*, larger diffusion coefficient), and ΔE_p decreases. The latter occurs because of a reduction in $\Delta G^{\ddagger}$. Preliminary data indicate that the carbon electrode microstructure influences the activation energy of this redox system in both [EMIM][BF_4] and [BMIM][BF_4]. For example, in the former RTIL, $\Delta G^{\ddagger}$ values (kJ/mol) in the less viscous [EMIM][BF_4] were 7.83 (BND) < 13.04 (t*a*-C:N) < 15.42 (GC), and in [BMIM][BF_4] were 24.43 (BND) < 28.93 (t*a*-C:N) < 34.23 (GC). These activation energies, particularly those for [BMIM][BF_4], are larger than those measured for a mechanistically complex aqueous redox system, $Fe(CN)_6^{-3/-4}$, at BND. At this electrode, $\Delta G^{\ddagger}$ ranged from 14.3-16.5 kJ/mol depending on the electrolyte (NaCl, KCl and CsCl). All electrodes were used in the "as received" state with not control over surface chemistry. Surface cleanliness was ensured by using a 20 min soak in ultrapure isopropanol; the typical pretreatment for BDD and t*a*-C:N electrodes

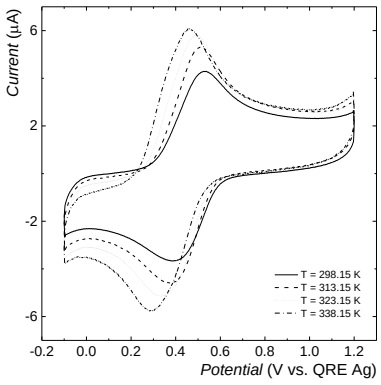

Figure 2. Cyclic voltammograms for 0.5 mM FCA in [BMIM][BF_4] as a function of temperature. Scan rate = 0.3 V/s. Electrode = t*a*-C:N.

Diffusion coefficients for the redox systems in the different RTILs were determined as a function of temperature (25-65 °C) from the cyclic voltammetric peak current-scan rate$^{1/2}$ relationship, and from chronoamperometric measurements (Cottrell analysis).

Heterogeneous electron-transfer rate constants were 1-2 orders of magnitude lower in RTILs than those typically observed for this and other ferrocene derivatives in aqueous electrolytes. Activation energies for electron transfer are 2x higher in the more viscous RTILs as compared with aqueous electrolyte solutions.

Table 1 presents a summary of data for D_R, k^o and E_a (activation energy for the ET reaction) for FCA in [BMIM][BF_4] and [EMIM][BF_4] at temperatures from 298-338 K. Very interesting is that the E_a for boron-doped nanocrystalline diamond is less in both ionic liquids that for GC or t*a*-C:N. E_a is larger in [BMIM][BF_4] than in [EMIM][BF_4] for all three electrodes likely because of the higher viscosity of the former, 112 vs. ~40 mPa-s. These values for E_a are significantly larger than the values seen in aqueous electrolytes (LiCl, NaCl, KCl) for $Fe(CN)_6^{3-/4-}$, 14-16 kJ/mol. The k^o values increase linearly with D_R. This finding indicates that the effects of temperature on mass transport (diffusion) and heterogeneous electron transfer follow the same law. These behaviors show possible solvent-dynamic control of the heterogeneous electron-transfer process with ET being coupled to diffusion.

Table 1. Diffusion coefficients and kinetics for FCA in [EMIM][BF_4] and [BMIM][BF_4] at different temperatures on various types of carbon electrodes.

Analyte/ solvent	Electrode	T, K	D_R, 10^{-7} cm^2 s^{-1}	k^0, 10^{-4} cm s^{-1}	k^0_{sim}, 10^{-4} cm s^{-1}	E_a, kJ mol^{-1}
FCA/	**GC**	298.15	1.30 ± 0.04	3.11 ± 0.87	5.23	15.42
[EMIM][BF_4]		313.15	1.76 ± 0.08	4.14 ± 0.24	6.87	(14.03*)
		323.15	2.02 ± 0.15	4.65 ± 0.40	7.12	
		338.15	2.10 ± 0.15	6.01 ± 0.38	9.26	
	BDD	298.15	1.84 ± 0.06	7.99 ± 0.34	14.80	7.31
		313.15	2.76 ± 0.09	8.90 ± 0.47	16.80	(8.87*)
		323.15	3.46 ± 0.13	9.48 ± 0.36	17.40	
		338.15	4.03 ± 0.11	10.71 ± 0.56	21.30	
	t*a*-C:N	298.15	1.52 ± 0.05	4.08 ± 0.41	6.96	13.04
		313.15	2.11 ± 0.09	5.25 ± 0.51	8.11	(9.98*)
		323.15	2.46 ± 0.11	5.92 ± 0.44	9.28	
		338.15	3.28 ± 0.26	6.72 ± 0.48	10.36	
FCA/	**GC**	298.15	0.68 ± 0.04	1.09 ± 0.28	3.00	34.23
[BMIM][BF_4]		313.15	1.23 ± 0.08	1.97 ± 0.15	4.09	(19.13*)
		323.15	1.65 ± 0.06	3.00 ± 0.52	5.21	
		338.15	2.59 ± 0.09	4.12 ± 0.49	6.23	
	BDD	298.15	0.24 ± 0.01	1.05 ± 0.21	2.89	24.03
		313.15	0.45 ± 0.01	1.42 ± 0.19	3.24	(11.13*)
		323.15	0.98 ± 0.02	1.99 ± 0.19	3.55	
		338.15	1.52 ± 0.02	2.68 ± 0.29	4.53	
	t*a*-C:N	298.15	0.71 ± 0.03	2.09 ± 0.33	4.11	28.93
		313.15	1.27 ± 0.08	3.29 ± 0.62	5.02	(15.03*)
		323.15	1.81 ± 0.05	4.88 ± 0.63	5.92	

	338.15	2.32 ± 0.18	6.71 ± 0.59	7.40

Diffusion coefficients and rate constants are reported as an mean ± standard deviation (n=3).
*Activation energy values calculated from the simulated cyclic voltammograms.

The larger activation barrier for ET in the ionic liquids could be due, in part, to a larger reorganizational energy barrier for the redox system. Since there is no solvent, it is possible that going from FCA to FCA^+ could involve considerable restructuring of the ionic liquid molecules around the molecule.

Several potential organic and inorganic redox systems were investigated as probes of the carbon electrode activity in RTILs. One promising molecule was the Fe-containing, hemin. The RTIL type appears to exert a strong influence on the voltammetric response at diamond. Two examples are presented below in Figure 3. In [BMIM][Otf(triflate)], a diffusion-controlled reaction is observed at boron-doped nanocrystalline diamond. Peak currents increase with the scan rate$^{1/2}$. 15% (v/v) of acetonitrile (ACN) was added to solubilize the molecule. The apparent heterogeneous electron-transfer rate constant, k^o_{app}, was found to be 4.5 x 10^{-3} cm/s. In contrast, in [BMIM][BF_4], also with 15% ACN added, adsorption behavior is observed with much lower peak currents. The adsorption on diamond is very unusual. Clearly, the IL structure can

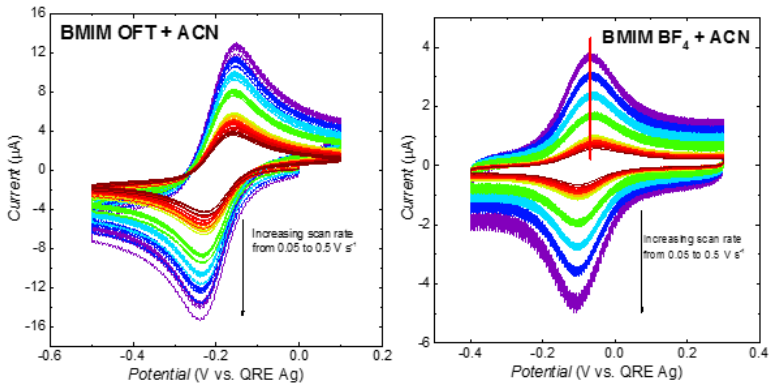

Figure 3. Cyclic voltammetric *i-E* curves for 0.5 mM hemin in (left) [BMIM][Oft] and (right) [BMIM][BF_4] at a BDD thin-film electrode. 15 % (v/v) acetonitrile added to both. Scan rates = 0.05 – 0.5 V/s.

exert a strong role on the reaction mechanism of a redox probe.

Specific Aim 3. Potential-Dependent Capacitance at the Two Carbon Electrode Materials as a Function of the RTIL Type and Electrode Surface Chemistry.
The goal of this aim was to determine the potential-dependent capacitance of BDD and ta-C:N thin-film electrodes in different RTILs as a function of the electrode microstructure and surface chemistry. Comparison studies were performed with glassy carbon.

Figure 4 shows background cyclic voltammograms for [BMIM][PF_6] at a BDD thin-film electrode as a function of scan rate. Curves are shown for 10, 30 and 100 mV/s after the ionic liquid was purified by a 50-min UHP Ar purge at 80 °C (so-called sweeping method). The currents increase proportionally with the scan rate indicative of capacitive processes. Calculated electrode capacitances range from 12-14 μF/cm^2. Capacitance values determined by voltammetric methods are usually a little higher than the true values because the current is not always purely capacitive. These values are comparable to what are found for the electrodes in 1M KCl or 0.5 M H_2SO_4. The concentration of ions in this IL is 4.2 M. Even though the dielectric constant is lower, the effective concentration is higher than the aqueous electrolytes so the capacitance values are similar in both electrolytes.

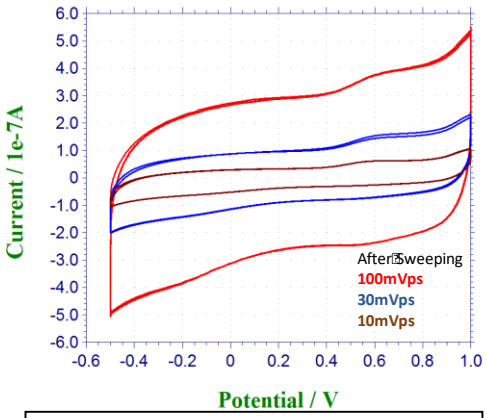

Figure 4. Cyclic voltammetric i-E curves for a boron-doped nanocrystalline diamond thin-film electrode in [BMIM][PF_6]. Ref.= Ag QRE.

Another important issue to address was how the interfacial capacitance changes with potential in RTILs at carbon electrodes of different microstructure and surface chemistry. Understanding how the RTILs wet the carbon electrode surface and how they organize at different potentials is important basic science to understand. There are two general models for explaining the interfacial double layer in ionic liquids. The first is the traditional Gouy-Chapman model, which is relevant for dilute electrolytes where the ions are sparsely distributed in the solvent. In this model a capacitance *minimum* is predicted near the point of zero charge (PZC). The second is based on the Poisson-Boltzmann lattice-gas model, more relevant for tightly packed ions with no solvent separation. In this model, a capacitance *maximum* is predicted near the PZC. The capacitance is predicted to decrease at potentials on either side of the PZC. Clearly, the organization of ions in an RTIL will be different from the organization in an aqueous electrolyte due to the absence of a dielectric solvent. Also, the viscosity of the RTIL will slow the ionic reorganization in response to a change in surface charge (E_{appl}-E_{pzc}). There is still a considerable amount that is unknown about the short- and long-range organization of RTILs, particularly at novel BDD and t*a*-C:N electrodes.

Table 2. Capacitance data in different RTILs.

	Capacitance, F cm^{-2} Recorded from CVs at 0.5 V		
Ionic liquid	**GC**	**BND**	**t*a*-C:N**
EMIM BF_4	7.18E-05	5.79E-06	2.36E-05
BMIM BF_4	8.97E-05	6.33E-06	1.31E-05
BMIM PF_6	9.04E-05	1.77E-05	2.81E-05
BMIM OTF	1.00E-04	1.92E-05	2.64E-05
HMIM BF_4	6.56E-05	1.73E-05	2.87E-05

The potential-dependent capacitance was measured three ways and compared: (i) cyclic voltammograms as a function of scan rate (10-100 mV/s), (ii) measuring the out-of-phase impedance as a function of potential at 0.1 or 1 Hz and calculating the capacitance using the following expression, $C = \frac{1}{2\pi f Z_{im}}$, and (iii) recording the entire impedance spectrum from 0.01 to 10,000 Hz as a function of the potential and determining the capacitance from fits to an equivalent circuit. All measurements were made at room temperature. Table 2 presents capacitance values at 0.5 V vs. Ag QRE for GC, BDD and t*a*-C:N electrodes in different RTILs. The general trends for these "as received" electrodes are GC > t*a*-C:N > BDD for all five RTILs. This trend is consistent with differences in the electronic properties (*i.e.*, density of electronic states) across the three materials.

Static contact angle measurements and XPS atomic O/C ratios for a BDD films treated in H_2, Ar and O_2 plasmas are shown in Figure 5. The H-terminated surface has the lowest O/C ratio (0.01) while the O-terminated surface has the highest ratio (0.17). The water contact angle is highest on the hydrophobic H-terminated surface (110°) and lowest on the hydrophilic O-terminated surface (41°). The opposite trend is seen for [BMIM][PF_6]. The RTIL wets the H-terminated surface with lower energy than the O-terminated surface. Figure 6 shows capacitance-potential data for these three functionalized BDD electrodes in [BMIM][PF_6]. A U-shaped capacitance- potential profile is seen for the H-terminated surface, consistent with the Gouy-Chapman model. The capacitance magnitude is largest for H-terminated diamond (lowest

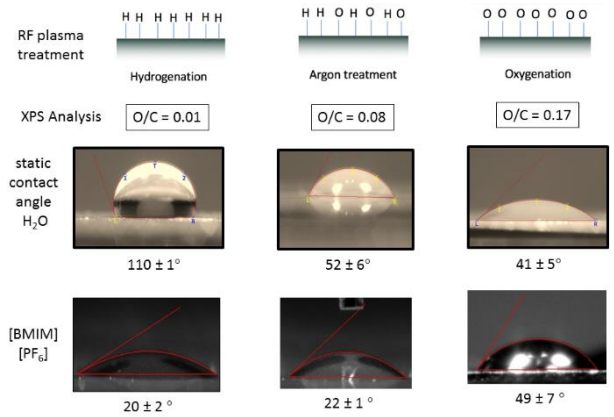

Figure 5. XPS and static contact angle data for H_2O and [BMIM][PF_6] at RF plasma-treated BDD electrodes.

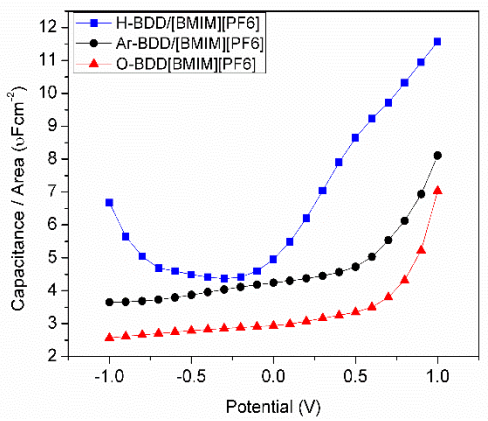

Figure 6. Capacitance-potential curves for a BDD thin-film electrode in [BMIM][PF_6]. Ref.= Ag QRE.

contact angle) and smallest for the O-terminated diamond (highest contact angle). It should be noted on some BDD and t*a*-C:N thin-film electrodes, capacitance maxima have been observed. Further research is needed to elucidate the factors that influence whether capacitance maxima or minima are observed in RTILs of different composition.

Data reveal that the capacitance-potential curves for a BDD thin-film electrodes are lower in a [HMIM][PF_6] – a larger organic cation. Values range from 5-6 μF/cm^2 over this potential range for the IL as received and 6-8 μF/cm^2 after the Ar sweeping. A capacitance minimum is seen in both ILs at ca. -0.7 V, which may be the point of zero charge in these media. We are continuing with studies of the capacitance in ILs of different cation types, [EMIM(ethyl)][PF_6], [BMIM(butyl)][PF_6] and [HMIM(hexa)][PF_6], and different anion types, [BMIM][BF_4] and [BMIM][PF_6]. These measurements are being made using GC, BDD and t*a*-C:N with surfaces low in oxygen (hydrogenated) and high in oxygen (O_2 plasma treatment). We want to learn what role the IL type and electrode surface chemistry has on the interfacial capacitance.

<u>Additional Research Accomplishments – Electroanalytical Applications</u>

Polyacrylamide-coated carbon nanotube (PA/CNT) electrodes were prepared by an ink-jet printing process and used to measure pyocyanin and uric acid in a wound fluid simulant at 37 °C. These two analytes are indicators of infection and could be useful biomarkers for monitoring wound healing. The long-term goal is to use these inexpensive and disposable electrodes to monitor biomarkers of healing in a wound environment. In this work, studies in a wound fluid simulant were performed to determine the stability of the electrodes and their responsiveness for the two analytes. The PA/CNT ink-jet printed electrodes and electrical contacts were stable with unchanging physical and electrochemical properties in the wound fluid simulant over a 7-8-day period at 37 °C. The detection figures of merit for pyocyanin in the simulant at 37 °C were as follows: linear dynamic range = 0.10 to 100 μM (R^2 = 0.9992), limit of detection = 0.10 μM (S/N =3), sensitivity = 35.6 ± 0.8 mA/mol L^{-1} and response reproducibility ≤ 4% RSD. The detection figures of merit for uric acid in the simulant at 37 °C were as follows: linear dynamic range at least from 100 to 1000 μM (R^2 = 0.9997), sensitivity = 2.83 ± 0.01 mA/mol L^{-1} and response reproducibility ≤ 4% RSD. The limit of detection was not determined. The PA/CNT electrodes were also used to measure pyocyanin concentrations in culture media from different strains of *Pseudomonas aeruginosa*. The detected concentrations ranged from 1.00 ± 0.02 to 118 ± 6 μM. (submitted *Anal. Chem*. **2018**).

The electroanalytical performance of a new commercial BDD disk and a traditional nanocrystalline thin-film electrode were compared for the anodic stripping voltammetric determination of Ag(I). The diamond disk electrode is more flexible than the planar film as the former is compatible with most electrochemical cell designs including those incorporating magnetic stirring. Additionally, mechanical polishing and surface

cleaning are simpler to execute. Differential pulse anodic stripping voltammetry (DPASV) was used to detect Ag(I) in standard solutions after optimization of the deposition potential, deposition time and scan rate. The optimized conditions were used to determine the concentration of Ag(I) in a NASA simulated potable water sample and a NIST standard reference solution. The electrochemical results were validated by ICP-OES measurements of the same solutions. The detection figures of merit for the disk electrode were as good or superior to those for the thin-film electrode. Detection limits were ≤ 5 µg L^{-1} (S/N=3) for a 120 s deposition period, and response variabilities were $< 5\%$ RSD. The polished disk electrode presented a more limited linear dynamic range presumably because of the reduced surface area available for metal phase formation. The concentrations of Ag (I) in the two water samples, as determined by DPASV, were in good agreement with the concentrations determined by ICP-OES (*Anal. Chem*. **2018**, *90*, 6477-6485).

Isatin is an anxiogenic indole and possesses anticonvulsant activity and has the potential to be an important ingredient in many future pharmaceutical applications. In this study, two electrode devices were fabricated and characterized. Furthermore, both devices were investigated for the detection of isatin. Each device comprised of a working, reference, and counter electrode, all made of boron-doped diamond. There were two different working electrode geometries, a 2 mm diameter macro electrode (MAC) and a microelectrode array (MEA); both devices used the same patterning for the reference and counter electrodes. The BDD quasi-reference electrode was studied by measuring its' potential against a traditional Ag/AgCl reference electrode and, while the potential changed as a function of solution pH, little potential drift was observed when holding the solution pH constant. Specifically, the BDD quasi-reference electrode had a potential -200 (vs. Ag/AgCl) in a solution pH of 7 and this remained stable for a 12-hour time period. For the detection of isatin, solutions were analyzed using both sensor configurations via the standard addition method in pH 7.4 phosphate buffered saline (PBS). Using the MEA sensor, the limit of detection (LOD, $\frac{3\sigma}{m}$) for isatin was found to be 0.04 µM; an increase to 0.22 µM was observed with the MAC sensor. These results were compared to the results obtained from a UV/Vis spectrophotometer where a 0.57 µM LOD was obtained. The results presented herein indicate that the MEA 3-in-1 device is applicable for low limits of detection. (*Anal. Chem.* **2018**, *90*, 1951-1958).

High pressure liquid chromatography (HPLC) with amperometric detection was used to quantify estrogenic compounds in water samples. The main goal was to compare the detection figures of merit for BDD and t*a*-C:N thin-film electrodes. The target analytes were estrone, estradiol, and estriol. The BDD and t*a*-C:N electrodes were investigated because of their excellent properties, which include a wide potential window, low background current, microstructural stability at high potentials, low limits of detection, weak molecular adsorption, fouling resistance and response reproducibility. t*a*-C:N electrodes have not yet been investigated extensively in electroanalysis and are receiving increasing interest because they exhibit many of the excellent electrochemical properties of BDD electrodes and they can be deposited at room temperature by physical vapor deposition. The results reveal as low or lower background current and noise for the t*a*-C:N electrode, as compared to the BDD electrode, and comparable or superior analytical detection figures of merit for all three emerging pollutants. The linear dynamic range for both electrodes was from 0.2 to 100 µmol L^{-1} for estriol, and 0.4 to 100 µmol L^{-1} for estradiol and estrone, and the sensitivity ranged from 9.1 to 11.2 mA mol L^{-1}. For all three analytes, the limit of detection (S/N=3) ranged from 0.16 – 0.35 µmol L^{-1} (45-95 ppb) for BDD and 0.20 – 0.34 µmol L^{-1} (58-95 ppb) for t*a*-C:N (*Electroanal.* **2018**, *30*, 1575-1582).

In an earlier article (*Langmuir*, **2016**, *32*, 9507-9512), we reported the existence of an induced charge density gradient, ρ_f, in a room temperature ionic liquid (RTIL, $BMIM^+BF_4^-$) normal to a charged planar silica surface. In this work, we demonstrate experimental control over the sign and magnitude of the gradient. The spatial extent of ρ_f can exceed 100 µm from the charged surface. We characterized ρ_f through the rotational diffusion time constant gradient of a cationic chromophore in the RTIL. The sign and magnitude of ρ_f in $BMIM^+BF_4^-$ is linked directly to the surface charge density of the electrode, which can

be controlled. We used transparent conductive electrodes (FTO and ITO coated on glass) as supports and demonstrated that control over the electrode surface charge carrier density can influence the magnitude and sign of ρ_f. There are limitations to this approach based on the FTO and ITO properties and we demonstrate these limits experimentally. (collaboration with Prof. Gary Blanchard, *J. Phys. Chem. C* **2018**, *122*, 7361-7367).

Isatin is an endogenous indole compound in humans and rodents that has a wide range of biological activity. In rat models, isatin concentrations have been shown to increase in the heart, brain, blood plasma, and urine with stress. Studies on patients suffering from Parkinson's disease have indicated a correlation between progress of the disease and urinary output of the molecule. Isatin is electrochemically active and can therefore be detected with electrochemical techniques. In this work, we compared the performance of a nitrogen-incorporated tetrahedral amorphous carbon (t*a*-C:N) and a BDD thin-film electrode for the oxidative detection of this biomolecule using flow injection analysis with amperometric detection. The measurements were performed in 0.1 phosphate buffer pH 7.2. The t*a*-C:N electrode, like boron-doped nanocrystalline diamond, exhibits some excellent properties for electroanalytical measurements including (i) low background current and noise, (ii) microstructural stability at positive detection potentials, and (iii) good activity for a wide range of bioanalytes without conventional surface pretreatment. The results reveal that both electrodes exhibit a linear dynamic range from 100 to 0.1 μmol L^{-1}, a short-term response variability 3-4% RSD (30 injections), a sensitivity of 18 mA M^{-1}, and a limit of detection (S/N=3) of 1.0 x 10^{-7} mol L^{-1} (14 ng mL^{-1} and 2.5 fmol) (*Electroanal.* **2017**, *90*, 2147-2154).

Manuscripts Published, In-Review or In-Preparation Acknowledging ARO Support

19. *The Potential Dependent Capacitance of ta-C:N Thin Film Electrodes in RTILs*. Bhardwaj K; Swain GM. JOURNAL OF THE ELECTROCHEMICAL SOCIETY (in preparation).
18. *Conductive Diamond: Synthesis, Properties and Applications*. Yang N; Yu S; Macpherson JV; Einaga Y; Zhao H; Swain GM; Jiang X. CHEMICAL SOCIETY REVIEWS (in press).
17. *Ionic Liquids. A Unique and Useful Class of Materials*. Ma K; Jarošová R; Wang Y; Swain GM; Blanchard GJ. THE CHEMICAL EDUCATOR (submitted).
16. *Surface Chemistry, Wettability and Capacitance of Chemically-Modified Boron-Doped Diamond Electrodes in RTILs.* Bhardwaj K; Swain GM. LANGMUIR (final preparation).
15. *Temperature Dependence of the Heterogeneous Electron-Transfer Rate Constant and Diffusion Coefficient for Ferrocene Carboxylic Acid in Room Temperature Ionic Liquids*. Jarošová R; Swain GM. JOURNAL OF PHYSICAL CHEMISTRY C (resubmitted).
14. *Ink-jet Printed Carbon Nanotube Electrodes for Measuring Pyocyanin and Uric Acid in a Wound Fluid Simulant and Culture Media*, Jarošová R; McClure SE; Gajda M; Jović M; Girault HH; Lesch A; Maiden M; Waters C; Swain GM. ANALYTICAL CHEMISTRY (submitted).
13. *Analysis of Ag(I) in Water Samples Using Anodic Stripping Voltammetry with a Boron-Doped Diamond Disk Electrode*, Maldonado VY; Espinoza PJ; Rusinek CA; Swain GM. ANALYTICAL CHEMISTRY 2018 (90) 1951-1958.
12. *Isatin Detection Using an All Boron-Doped Diamond 3-in-1 Macro Electrode and Micro Electrode Array*, Ensch M.; Maldonado VY; Rusinek CA; Swain GM; Rechenberg R; Becker MF; Wehring B, Schuelke T. ANALYTICAL CHEMISTRY 2018 (90) 1951-1958.
11. *HPLC-EC Analysis of Estrogenic Compounds Using Tetrahedral Amorphous Carbon Thin-Film Electrodes*, Espinoza E.; Jarosova R.; Swain GM, ELECTROANALYSIS 2018 (30) 1575-1582.
10. *Modulation of an Induced Charge Density Gradient in the Room Temperature Ionic Liquid $BMIM^+BF_4^-$*, Ma K; Jarosova R; Swain GM; Blanchard GJ. JOURNAL OF PHYSICAL CHEMISTRY C 2018 (122) 7361-7367.
9. *Isatin Analysis Using Flow Injection Analysis with Amperometric Detection: Comparison of Tetrahedral Amorphous Carbon and Diamond Electrode Performance*. Jarosova R; Sanchez S; Haubold L; Swain GM. ELECTROANALYSIS 29 (2017) 2147-2154.
8. *Charge-Induced Long Range Order in a Room Temperature Ionic Liquid*. Ma K; Jarosova R; Swain

GM; Blanchard GJ. LANGMUIR 32 (2016) 9507-9512.

7. *Evaluation of Nitrogen-Incorporated Tetrahedral Amorphous Carbon Thin-Film for the Detection of Tryptophan and Tyrosine Using Flow Injection Analysis with Amperometric Detection*. Jarosova R.; Rutherford J; Swain GM. ANALYST 141 (2016) 6031-6041.
6. *Assessment of Heterogeneous Electron-Transfer Rate Constants for Soluble Redox Analytes at Tetrahedral Amorphous Carbon, Boron-Doped Diamond and Glassy Carbon Electrodes*. Jarosova R; De Sousa Bezerra PM; Munson C; Swain GM. PHYSICA STATUS SOLIDI A: APPLICATIONS and MATERIALS SCIENCE (special issue on Novel Aspects of Diamond) 213(2016) 2087-2098.
5. *Structure, Electronic Properties and Electrochemical Behavior of a Boron-Doped Diamond/Quartz Optically Transparent Electrode*, Wachter N.; Munson C; Jarosova R; Berkun I; Hogan, T; Rocha-Filho R; Swain GM. ACS APPLIED MATERIALS and INTERFACES 8 (2016) 28325-28337.
4. *Effects of Film Morphology and Surface Chemistry on the Direct Electrochemistry of Cytochrome c at Boron-Doped Diamond Electrodes.* Dai Y; Proshlyakov DA; Swain GM. ELECTROCHIMICA ACTA 197 (2016) 129-138.
3. *Nanocarbon Electrochemistry and Electroanalysis: Current Status and Future Perspectives.* Yang N; Swain GM; Jiang X. ELECTROANALYSIS (Special Issue) 28 (2016) 27-34.
2. *Rapid Preparation of Room Temperature Ionic Liquids with Low Water Content as Characterized with a ta-C:N Electrode*. Jarosova R; Swain GM. JOURNAL OF THE ELECTROCHEMICAL SOCIETY 162 (2015) H507-H511.
1. *Diamond Electrodes: Diversity and Maturity.* Einaga, Y; Foord JS; Swain GM. MRS BULLETIN 39 (2014) 525-532.